

Multiple-Wavelength Holographic Interferometry

David C. Weber, Neal J. Brock, James D. Trolinger, and James E. Millerd

MetroLaser, Inc., 18006 Skypark Circle, Suite 108, Irvine, California 92614

A number of interesting and useful interferometric measurements can be obtained by using more than one wavelength. The following report discusses how holography enhances both the possibilities and results obtained from multiple-wavelength interferometry. A discussion of approaches is followed by a number of examples from our own laboratory work in this area. In the first example, two widely separated wavelengths are employed to exploit the dispersive properties of a solution to measure temperature and concentration simultaneously. In this case holographic recording makes phase-shifting interferometry possible with a snapshot recording. In the second example, the use of anomalous dispersion at the resonance of a gas is exploited to measure species concentration. This is accomplished by direct optical subtraction of the two different wavefronts, one at resonance and the other off resonance. Finally, two closely spaced wavelengths are reflected from a diffuse surface and subtracted optically by holography to contour a surface.

Journal of Imaging Science and Technology 41: 342–354 (1997)

Introduction

The use of holography has been shown to provide tremendous enhancement to interferometry, enabling many new types of measurements that cannot be otherwise achieved.^{1–3} In this report we address some of the specific features of holography that can be applied to enhance interferometry, particularly as it relates to the use of multiple wavelengths and we provide specific examples from our own work that demonstrate new types of multiple-wavelength measurements.

Most types of interferometry quantify and compare wavefronts by combining a spherical or collimated reference wavefront with the data wavefront to produce interference fringes (the interferogram) that can be interpreted in terms of the phase of the data wavefront.⁴ The data wavefront is produced by passing light through a field of interest or reflecting it from a surface to pick up phase information that depicts either changes in refractive index or some movement of the surface. Measures must be taken to ensure that all optical components and windows are of extremely high quality and free of contaminants to prevent the introduction of phase changes that add ambiguity to the phase information generated by the actual phenomenon being studied. Such imperfections in the path of either the reference or object waves introduce phase modulations that show up as unwanted fringes or fringe modulations in the interferogram that, at best, are an annoyance and, at worst, can confuse or completely obscure legitimate data. In addition, if the phase variations in the object field or surface under inspection are large or complex, the resulting fringe density can be so large as to make any reasonable data interpretation impossible.

The use of holography greatly enhances the reduction of unwanted phase noise as well as allowing for the interpretation of extremely complex wavefronts. In holography,

a coherent wavefront of arbitrary complexity is recorded onto a photosensitive media by combining it with a simple reference wavefront. The interference pattern formed by the two wavefronts allows both the intensity and phase of the object wavefront to be saved and reconstructed on demand when the hologram is reilluminated with a reconstruction wave sufficiently similar to the original reference wave used during recording. In holographic interferometry, the reconstructed wavefront is combined with a second wavefront of the same subject or test cell after some change has occurred. This second wavefront may be a live scene or another holographic reconstruction. In either case, both wavefronts experience the same optical path and pass through and/or reflect off the same optical components. Thus, only differences in the subject itself produce interference fringes, no matter how complex the individual wavefronts may be. Because both wavefronts pass through the same optical path, this approach also relaxes the requirement for high-quality lenses, windows, and mirrors.

Holography offers other enhancements to the field of interferometry. Techniques that improve the sensitivity and accuracy of interferometry, such as phase-shifting interferometry (PSI),⁵ heterodyne interferometry (HI),^{6,7} and resonance interferometry (RI),⁸ can be further enhanced and implemented in unusual and powerful forms by incorporating holography. Finally, holography allows for the use of multiple-wavelength interferometry, in some cases leading to measurements that have no obvious equivalent in conventional interferometry. This last enhancement of holography to the field of interferometry is the focus of the present report.

In summary, the application of holography to interferometric measurements leads to many possibilities and enhancements including:

1. System imperfections are canceled because both wavefronts that form the interferogram experience the same imperfections.
2. Object properties (no matter how complicated) that affect wavefronts that are fixed in time can be holographically recorded and optically subtracted from other similar wavefronts.

Original manuscript received December 12, 1996.

©1997, IS&T—The Society for Imaging Science and Technology

3. Wavefronts that existed at different times can be stored holographically, reconstructed later, then added or subtracted (or processed in other ways).
4. PSI and HI can be performed on a reconstructed wavefront recorded from an instant in time with a pulsed laser. (PSI and HI normally require time for introducing phase shifts and cw lasers.)
5. Wavefronts from two mutually incoherent lasers can be stored holographically then reconstructed and interfered later at a single wavelength, effectively allowing interferometry of two different wavelengths.

Multiple-Wavelength Holography

The use of a second wavelength via holography introduces a number of interesting interferometric measurements. Multiple-wavelength holographic interferometry requires sources at different wavelengths, recording material that can record holograms at each wavelength, and a reconstruction procedure that allows accessing the two reconstructed waves in a useful manner. A wide range of possibilities are available to produce two or more wavelengths suitable for multiple-wavelength holographic interferometry. Large wavelength separations of up to many hundreds of nanometers can be achieved using either two separate lasers (e.g., two tunable dye lasers) or one multiple-wavelength laser (e.g., doubled YAG or argon). Single laser sources (e.g., Zeeman or diode) can also be used to produce smaller wavelength separation. Other methods for attaining smaller frequency (wavelength) separations ranging from a few kilohertz to a few gigahertz include lasers with special etalons, tunable diode lasers, Bragg cells, and reverse Brillouin scattering cells.⁹⁻¹¹

The second wavelength can be used in one of three ways: First, the two wavelengths can be used to create two interferograms that are each analyzed separately. The dispersive properties of a test material are utilized to provide new, independent diagnostic data at the second wavelength. For example, when both temperature and concentration affect the refractive index of a solution, the second wavelength can be used to separate these effects. A large wavelength separation is typically required to make such a measurement useful. A specific case where a large separation is not required, however, is near a resonance line of a material where anomalous dispersion causes a drastic change in phase information for a small change in wavelength.

Second, the two wavelengths can be interfered to produce a third, so-called synthetic (or beat) wavelength that is used as a diagnostic. For instance, HI can be used to measure optical path length with resolutions better than $\lambda/10,000$.¹²⁻¹⁴ If the difference between the two wavelengths $\Delta\lambda$ is much smaller than the average wavelength λ , then the synthetic wavelength λ_s is given by

$$\lambda_s = \lambda^2 / \Delta\lambda.$$

If either of the two interfering waves is phase shifted, the synthetic wavelength is likewise shifted by the same amount. Because the frequency of the synthetic wave is much lower, phase shifts can be detected and measured electronically in an extremely precise manner. The phase of the synthetic wavelength can thereby be accurately correlated to the relative phase of the two waves, because the change in relative phase of the two waves is followed by the equivalent change in phase of the synthetic wavelength.

This approach can be altered slightly for use in optical profilometry, where the synthetic wavelength is used to measure large profile deviations that would produce far too many fringes to be measurable using single wavelength interferometry. The synthetic wavelength in this case desensitizes the measurement system to depth changes. Many of the advantages of holography outlined in the **Introduction** can be exploited in profilometry. In particular, real-time holographic interferometry can be used to measure the relative changes in the profile of a part or surface.⁹ Traditional interferometry can generally only measure absolute changes, because the wavefront owing to the surface profile is compared to a simple collimated or spherical wavefront.

The third manner of utilizing the second wavelength is to directly interfere it with the first. This concept is unique to holographic interferometry, because this type of interference does not even have definition in traditional interferometry. Holography, therefore, provides unique and powerful methods for interfering mutually incoherent wavefronts. When holograms are recorded at two wavelengths and played back at a single wavelength, two reconstructed waves emerge at different angles that depend on the recording geometry and the wavelength difference. If the two wavefronts are to be used interferometrically, the angle must be small. If the recording subject and reference beams are the same for both wavelengths, then the reconstructed waves will be nearly congruent only if the wavelength separation is small. The recording geometry can be chosen such that the two wavefronts emerge at the same angle or with any desired angle between them. This can be achieved by using separate recording and reconstruction reference waves for the two wavelengths and properly choosing the reconstructing wavelength. Reconstructing at wavelengths that differ from recording wavelengths, however, introduces chromatic aberrations that are especially limiting when different reference wave angles are used. A holographic correcting method has been developed in our studies to record wavefronts at two different wavelengths and thus achieve the simultaneous, congruent, corrected reconstruction of the two at an arbitrary third wavelength.¹⁵ The reconstruction is achieved with wavefronts generated by another hologram. The method automatically corrects aberrations and aligns the reconstructed wavefronts for interferometry.

An important example of this unique implementation of holographic interferometry is resonant holographic interferometry (RHI). In this application, one of the wavelengths is selected to correspond to a resonance of a particular species of interest in a flow field. Anomalous dispersion of the target species results in extremely large values of refractive index at the resonance wavelength. The phase of a wavefront is, therefore, dramatically altered by the presence of the target species. The concentration of that species can, therefore, be separated from all other constituents in the flow field, which produce very little phase shift in the wavefront.

In the following sections, three examples of our work at MetroLaser, Inc., in the area of multiple-wavelength holographic interferometry are presented:

1. Two widely separated wavelengths are employed to exploit the dispersive properties of a solution to provide additional diagnostics data. Holographic recording makes phase-shifting interferometry possible with a snapshot recording.
2. Anomalous dispersion at the resonance of a gas is exploited to measure species concentration. Holographic

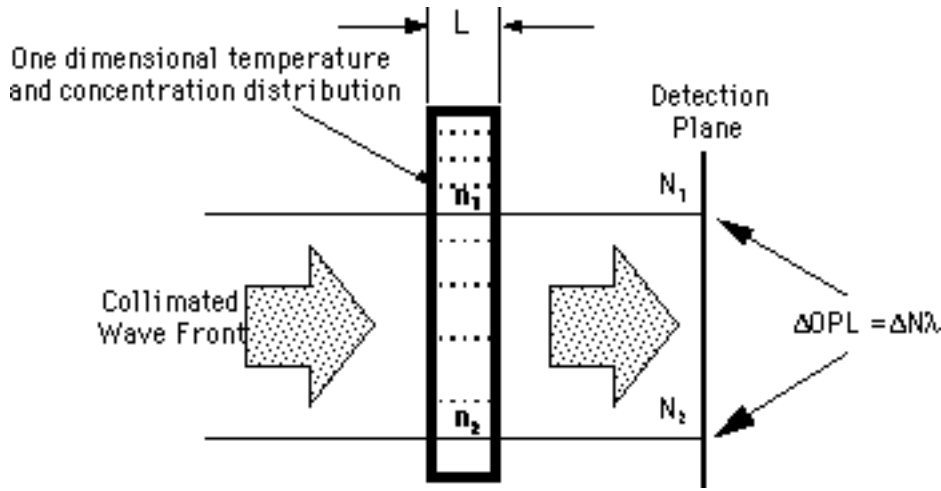


Figure 1. Application of TCHI to a test cell with one-dimensional temperature and concentration distributions.

recording enables direct optical subtraction of the two different wavefronts.

3. Two closely spaced wavelengths are reflected from a diffuse surface and subtracted optically by holography to contour a surface. These last two cases employ real-time holographic recording with nonlinear optical materials.

Theoretical Background

Two-Color Holographic Interferometry (Simultaneous Measurement of Solution Temperature and Concentration). Two-color holographic interferometry¹⁶ (TCHI) is a technique that utilizes the independent effects of two parameters, such as solution temperature and concentration, on the refractive index of a solution. Because both parameters affect the refractive index of the solution, single-color interferometry cannot be used to separate the two effects. By using two wavelengths, two independent interferograms provide the additional independent equation required to determine the two unknowns. Early work using this method was done to measure temperature and concentration of fuel mixtures, where the refractive index and dispersion were very high.¹⁷ Ecker has also used the technique to make similar measurements in alloy solidification.^{18,19} Another important application of the technique is in the area of crystal growth from solutions, where concentration gradients in the growth solution must be carefully monitored. While the technique is straightforward in principle, the sensitivity of the technique to small errors in a number of parameters must be addressed before it can be used successfully.

A typical TCHI configuration is shown in Fig. 1. A test cell with a solute in solution has one-dimensional gradients in both temperature and concentration. Two beams from a collimated wavefront of coherent light pass through the test cell. An interferogram is made by combining this wavefront with one from a hologram made of the same test cell containing a solution at constant temperature and concentration throughout the volume. The measured phase of each beam is the difference between the wavefront passing through the “live” test cell and that from the hologram recorded earlier. If the refractive index of the solution during recording of the hologram was n_1' , the optical path lengths (OPLs) of the top beam for the live and holographically recorded wavefront over the entire path, s_1 , are:

$$\text{OPL}_{1,\text{live}} = \text{OPL}_{\text{out sol}} + Ln_1,$$

$$\text{OPL}_{1,\text{holo}} = \text{OPL}_{\text{out sol}} + Ln_1',$$

where L is the cell thickness. The relative change in OPL between the live and recorded conditions are,

$$\Delta\text{OPL}_1 = \text{OPL}_{1,\text{live}} - \text{OPL}_{1,\text{holog}} = L(n_1 - n_1'), \quad (1)$$

assuming that nothing in the optical path outside the solution has changed. Similarly, for the bottom beam,

$$\Delta\text{OPL}_2 = \text{OPL}_{2,\text{live}} - \text{OPL}_{2,\text{holog}} = L(n_2 - n_2'). \quad (2)$$

Because the hologram was made for constant temperature and concentration, $n_1' = n_2' = n'$. Putting Eqs. 1 and 2 in terms of fringe order, $N (= \text{OPL}/\lambda)$, we get,

$$\Delta N_1 = L(n_1 - n') / \lambda, \quad (3)$$

$$\Delta N_2 = L(n_2 - n') / \lambda. \quad (4)$$

If the refractive index n_1 is taken as a reference condition, the refractive index n_2 in terms of n_1 can be related to changes in temperature and concentration between these two points by the relation,

$$n_2 = n_1 + \left(\frac{\partial n}{\partial c}\right)\Delta c + \left(\frac{\partial n}{\partial T}\right)\Delta T, \quad (5)$$

where Δc and ΔT are the changes in concentration and temperature between the two points, $\partial n/\partial c$ and $\partial n/\partial T$ are properties of the solution that depend on the wavelength of the illuminating beam as well as solution temperature and concentration. Combining Eqs. 3 and 4 with this relation gives

$$\frac{\Delta N\lambda}{L} = \left(\frac{\partial n}{\partial c}\right)\Delta c + \left(\frac{\partial n}{\partial T}\right)\Delta T, \quad (6)$$

where $\Delta N = \Delta N_2 - \Delta N_1 = L(n_2 - n_1) / \lambda$. because of dispersion within the solution, $\partial n/\partial c$ and $\partial n/\partial T$ are different at different wavelengths. This relation can be used, therefore, at two different wavelengths to create a set of two independent equations:

$$\frac{\Delta N_j \lambda_j}{L} = \left(\frac{\partial n}{\partial c} \right)_j \Delta c + \left(\frac{\partial n}{\partial T} \right)_j \Delta T, \quad (7)$$

$$\frac{\Delta N_k \lambda_k}{L} = \left(\frac{\partial n}{\partial c} \right)_k \Delta c + \left(\frac{\partial n}{\partial T} \right)_k \Delta T, \quad (8)$$

where i and j denote the two different wavelengths. Solving for Δc and ΔT gives

$$\Delta c = \frac{\Delta N_j \lambda_j \left(\frac{\partial n}{\partial T} \right)_k - \Delta N_k \lambda_k \left(\frac{\partial n}{\partial T} \right)_j}{L \left[\left(\frac{\partial n}{\partial c} \right)_j \left(\frac{\partial n}{\partial T} \right)_k - \left(\frac{\partial n}{\partial c} \right)_k \left(\frac{\partial n}{\partial T} \right)_j \right]}, \quad (9)$$

$$\Delta T = \frac{\Delta N_j \lambda_j \left(\frac{\partial n}{\partial c} \right)_k - \Delta N_k \lambda_k \left(\frac{\partial n}{\partial c} \right)_j}{L \left[\left(\frac{\partial n}{\partial T} \right)_j \left(\frac{\partial n}{\partial c} \right)_k - \left(\frac{\partial n}{\partial T} \right)_k \left(\frac{\partial n}{\partial c} \right)_j \right]}, \quad (10)$$

where Δc and ΔT are the changes in concentration and temperature from the reference condition, L is the width of the test cell, and N is the fringe order.

Resonant Holographic Interferometry (Species Identification and Distribution). Unlike TCHI, resonant holographic interferometry (RHI) uses two wavelengths that are very close together. RHI provides a method for obtaining species specific interferograms by recording two simultaneous holograms in which one of the wavelengths is tuned near a chemical absorption feature and the other tuned off this feature (typically < 0.1 nm separation between lasers).^{20,21} Because phase contributions to the interferogram from background species, thermal and pressure gradients, and optical aberrations are subtracted out in the holographic reconstruction process, the resulting interference fringes correspond uniquely to the density of the species under interrogation. The interferogram permits two-dimensional chemical detection that is useful for combustion and plasma diagnostics, medical imaging, and flow visualization. Real-time RHI has recently been demonstrated using a bacteriorhodopsin (BR) polymer thin film as the recording medium; however, the long lifetimes of BR in the polymer host limited²² the interferogram acquisition rate to 1 Hz.

The use of photorefractive semiconductors extends the current RHI technology into the near-infrared (NIR) spectral region, where conventional holographic recording media are unavailable, and enables real-time measurement capability. The NIR region is easily reached with inexpensive, commercially available laser diodes. In addition, laser diode output can be easily coupled into single-mode fiber optic cables that greatly reduce the size and complexity of the optical delivery system by eliminating multiple beam steering mirrors and periscopes. Holographic images can be recorded, reconstructed, and erased in photorefractive semiconductors on time scales less than 10 ns, making it possible to achieve megahertz data rates.²³

Photorefractive crystals²⁴⁻²⁸ such as $\text{Bi}_{12}\text{SiO}_{20}$, $\text{Bi}_{12}\text{TiO}_{20}$, and LiNbO_3 have been used to replace conventional films, allowing in situ exposure, development, and erasure of holographic interferograms; however, these ferroelectric oxides often show very slow or no response at the NIR wavelengths of commercial laser diodes. Vanadium-doped zinc telluride ($\text{ZnTe}:\text{V}$) has demonstrated²⁹ fast photorefractive response in the spectral range of 0.6 to 1.3 μm . The figure of merit corresponding to the electro-optic in-

dex change per separated charge suggests that ZnTe has the highest sensitivity of the known photorefractive semiconductors.³⁰

Two-Color Contour Holography (Variable Sensitivity Contour Mapping). Holographic contouring is an established technique for measuring surface profiles of optically rough surfaces.^{31,32} As in RHI, the two wavelengths are chosen very close to one another (typically < 0.3 -nm separation) to create a so-called synthetic wavelength less sensitive to depth changes. Contour maps are generated by interfering two holographic images recorded at different wavelengths, resulting in an interference pattern that corresponds to planes of constant elevation relative to a reference plane. This plane can be chosen so that it corresponds to the direction normal to the image plane. If the two reconstructed holographic images of an object are interfered (each recorded at a different wavelength), the intensity of the interferogram at any one point (x,y) is given by²:

$$I(x,y) = A(x,y) + B(x,y) \cos \left(\frac{4\pi \cdot \Delta z(x,y)}{\lambda_s} + \phi \right), \quad (11)$$

where

$$\lambda_s = \frac{\lambda^2}{\Delta \lambda} \cos \alpha = \frac{c}{\beta \Delta i} \cos \alpha \quad (12)$$

is the synthetic wavelength; $A(x,y)$ and $B(x,y)$ are constants related to the intensity of scattered light from the object; λ is the nominal operation wavelength; $\Delta \lambda$ and $\Delta \nu$ are the wavelength and frequency difference between recordings, respectively; c is the speed of light; Δz is the change in object elevation with respect to an arbitrary plane; α is the half-angle between the illumination and viewing angles; ϕ is an arbitrary phase angle; Δi is the change in the drive current; and β is the so-called current-frequency modulation index. For our diode, a change in current of 25 mA produces a contour interval of 2 mm. With established fringe analysis software, a contour resolution of 40 μm can be obtained (assuming a fringe resolution of 1/50 typical of phase-shifting interferometry).

This technique is a well-known whole-field measurement for profiling optically rough surfaces.² To construct a robust, practical instrument, it is necessary to acquire data quickly, incorporate a compact laser source, and integrate quantitative data reduction. Kuchel and Tiziani³³ demonstrated real-time two-color contour holography with a BSO photorefractive crystal in a four-wave mixing geometry with fixed wavelengths from a krypton laser. Recently it was demonstrated that a compact diode laser could be frequency tuned and used with electronic holography to obtain 3-D depth profiles.^{34,35} Photorefractive crystals provide higher spatial resolution than that currently available with electronic holography; however, until recently,³⁶ photorefractive response at the near-infrared wavelengths of laser diodes was poor.

In our work at MetroLaser, Inc., we have combined the use of a diode laser and a photorefractive crystal [rhodium-doped barium titanate ($\text{BaTiO}_3:\text{Rh}$)] to demonstrate an extremely robust, compact, and flexible instrument. Interferograms were produced with a depth contour interval that could be continuously tuned in real-time by adjusting the drive current of the diode. The high gain coefficient of BaTiO_3 made use of applied fields unnecessary, and the

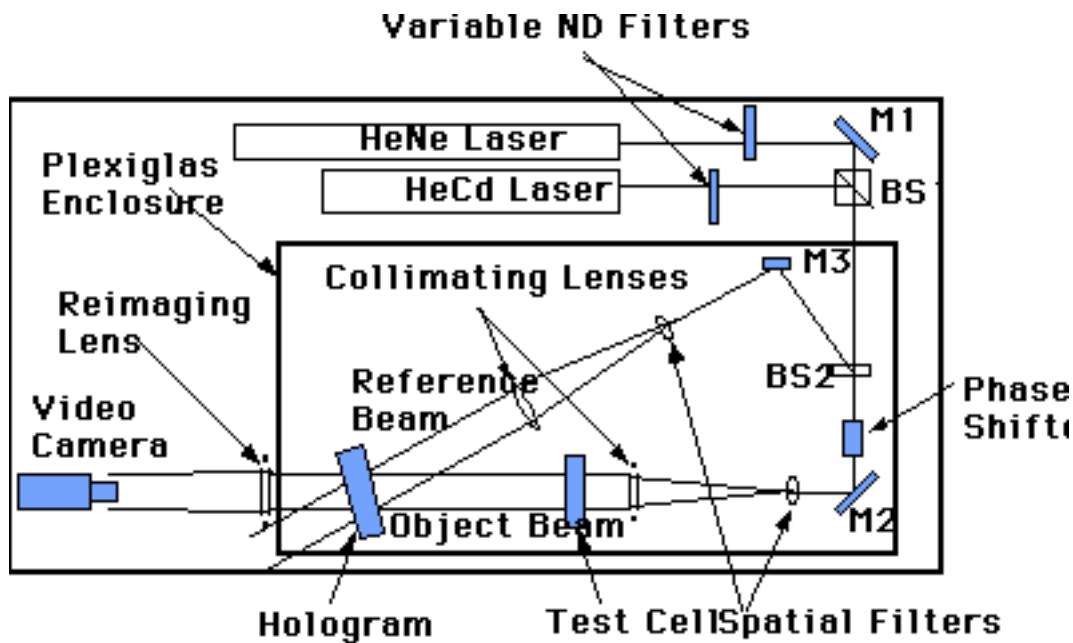


Figure 2. Experimental setup for two color holographic interferometry.

two-wave mixing geometry resulted in a compact architecture. The ability to produce multiple contour intervals is a significant advancement because it permits incorporation of a newly developed, fast data processing algorithm that produces quantitative depth profiles, handles step discontinuities, and is suitable for parallel processing.³⁷

Experimental Results

Experimental studies have been performed at Metro-Laser, Inc., for each of the three techniques outlined in the previous section. A brief description of the experiments carried out will be described below along with some of the more interesting results and observations in each case. The results outlined here not only demonstrate the power of utilizing two-color techniques, but show the diversity of measurements possible.

Two-Color Holographic Interferometry. A diagram of the breadboard in the TCHI experiments is shown in Fig. 2. Light for the two colors was provided by a HeNe laser ($\lambda = 632.8 \text{ nm}$) and HeCd laser ($\lambda = 441.6 \text{ nm}$). These lasers were selected to maximize the amount of dispersion for the TCHI demonstration. The beams from the two lasers were combined using a cube beamsplitter BS1 and split into reference and object beams with BS2, which was a variable beamsplitter. Each beam contained both colors and was spatially filtered and collimated. The object beam passed through a specially built test chamber designed to allow a high degree of control over the temperature and concentration gradients produced in the test cell contained in the chamber. Using this setup, a hologram was made and then placed back into the hologram holder. Interferograms were formed by combining light passing through the test section (object beam) with the reconstructed image of the test cell (reference beam). Reimaging optics were used to image the test cell onto a CCD array.

PSI was used to reduce the data using a piezoelectric phase shifter to control the phase shift between the interferograms. This allowed the data to be obtained for each laser in less than a second, which was important to en-

sure that random phase shifts, such as caused by wind currents, were not introduced between each phase shift.

Interferograms were formed by combining the hologram of the test cell with the live cell. Initially the live cell was unmodified from its condition when the hologram was recorded. This permitted minor adjustments in the plate position after chemical processing so that an "infinite fringe" condition could be obtained. The ideal infinite fringe interferogram could not be obtained at that time, but by digitizing the interferogram obtained, corrections could be made to later interferograms made with a live test cell containing temperature and/or concentration gradients. In this manner, the interferogram is essentially normalized to the infinite fringe condition.

The interferograms used in the TCHI method were produced by interfering a live (real-time) wavefront passing through a test cell containing temperature and concentration gradients with a wavefront reconstructed from a hologram of the same test cell with no gradients (i.e., constant temperature and concentration). To a first order, the only differences in the two wave fronts interfered were the changes in temperature and concentration; however, many second-order effects were also found that severely affected the test results including nonuniform shrinkage of the photographic emulsion on which the hologram was recorded, slight misalignment of the processed hologram from the position it was recorded in, and magnification differences between the two colors owing to achromatic aberrations in the camera imaging system. A reference interferogram to compensate for these errors was made by interfering the holographically recorded image of the test cell containing no temperature or concentration gradients with the live cell under the same conditions. The phase variations contained in this interferogram were subtracted from subsequent interferograms resulting from the addition of temperature and/or concentration gradients.

Typical interferograms for a test cell containing both temperature and concentration gradients is shown in Fig. 3 for red and blue light, respectively. The center portion with the nearly horizontal fringes is the test cell where

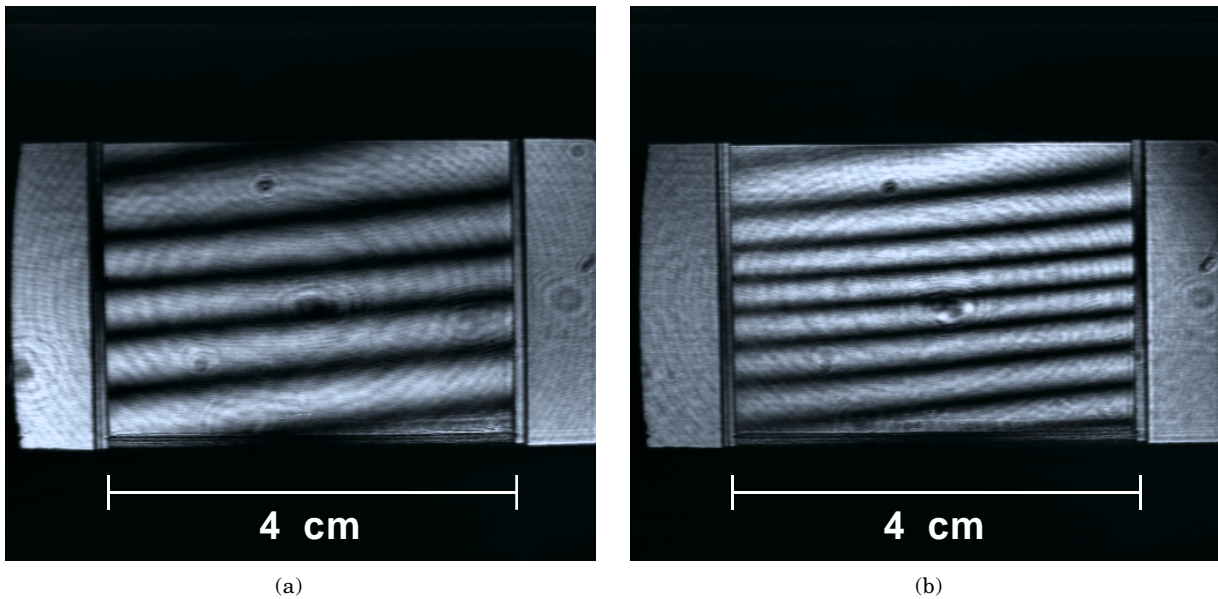


Figure 3. Interferograms of the test cell containing both temperature and concentration gradients, (a) using red, HeNe laser illumination ($\lambda = 632.8$ nm) and (b) using blue, HeCd laser illumination ($\lambda = 441.6$ nm).

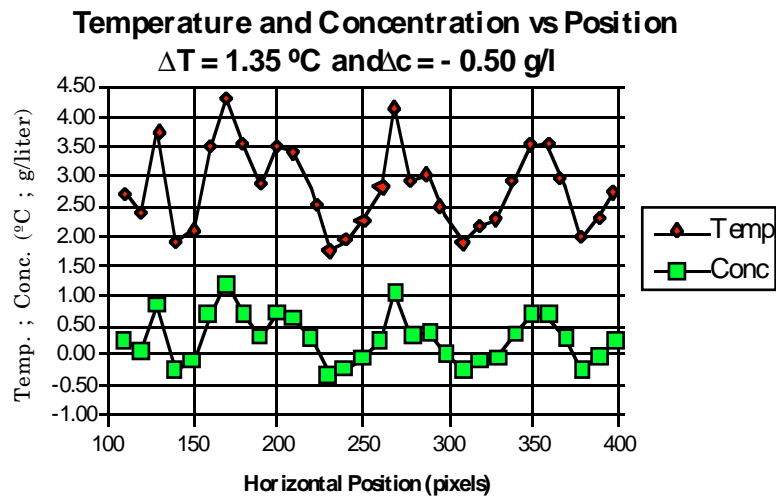


Figure 4. TCHI results using raw phase data.

various temperature and concentration gradients were set up. The areas of nearly constant intensity to either side of the horizontal fringes are the air gaps to either side of the test cell. The gradual change in intensity from top to bottom indicates a very slight tilt of the hologram about the horizontal axis. This tilt had to be subtracted out of the phase measurements made in the test cell to obtain the correct result for ΔT and Δc . Several corrections in the phase data were required before successful results could be obtained. These corrections included tilt in the hologram plate, phase information introduced by the hologram plate and emulsion, and chromatic aberrations introduced by the imaging optics.

Figure 4 shows the results of applying the TCHI equations to the raw phase data. This figure demonstrates the instability of the TCHI equations when the sources of phase error cited above are not taken into account. Note that even in this case, the correct value of Δc is calculated at data points where the correct value of ΔT resulted from the phase measurement. This gave us the initial confi-

dence that the correct answer was contained in the phase data, even though the initial results looked so chaotic.

Figure 5 shows the results for various test cell conditions when phase data are corrected using the reference interferogram as explained above. Variations in the calculated values of ΔT and Δc across the cell are even smaller now, with the average value being very close to that measured by independent means. On average, the TCHI method gave the correct value of ΔT and Δc to within 0.2°C and 0.15 g/l, respectively. The variation in the calculated values of ΔT was $\pm 0.14^\circ\text{C}$ to $\pm 0.27^\circ\text{C}$, while Δc variations were between ± 0.06 to ± 0.19 g/l.

The expected error of the measurements of ΔT and Δc using the TCHI technique, based on uncertainties in the ΔN measurement and on the temperature and concentration conditions of the solution, were found to be about 0.11°C and 0.08 g/l, respectively. These numbers represent the average error expected in calculated values of ΔT and Δc based on the given measurement error in ΔN . Variations in the derived values of ΔT based on the TCHI phase

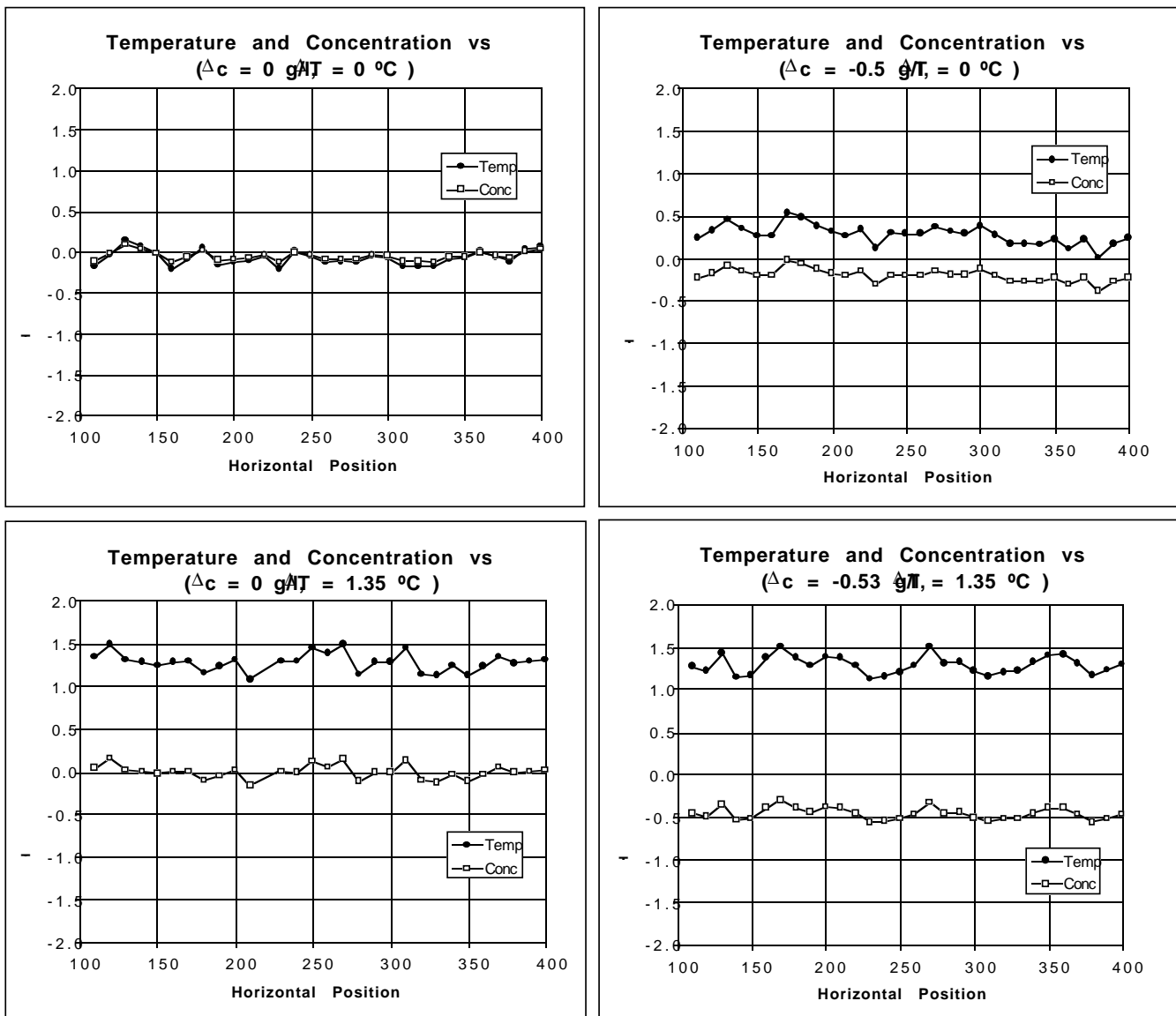


Figure 5. TCHI results when all phase corrections are made to interferograms.

measurements were between 0.05°C and 0.18°C , while for Δc the variations were between 0.04 and 0.12 g/l. This shows a remarkable correlation to the predicted results and demonstrates the capability of the analytical error analysis to predict how well the TCHI method will work in a particular set of circumstances. The average error in the ΔT and Δc readings from the actual values was about 0.07°C and -0.05 g/l (or 5.4% and -9.8%). Statistically, for a sampling of 30 data points (the case for these interferograms), the average error might be expected to be smaller. This discrepancy can be attributed to inaccuracies in the independent measurements of ΔT and Δc and some systematic, unaccounted for, error in the phase measurements. The results were extremely good, given the many corrections implemented into the raw data.

Resonant Holographic Interferometry. The conceptual design for our real-time RHI system is shown in Fig. 6. The laser beams tuned to the on- and off-resonance wavelengths are s-polarized, pass colinearly through the test object (combustion flow field, plasma reaction chamber, etc.), and are focused down to match the crystal aper-

ture. Two reference beams are also colinear and s-polarized. By properly selecting the wavelengths and geometry, phase conjugate replicas of both object beams produce interference fringes at the detector plane that correspond to the density of the species under interrogation. The polarization rotational properties of four-wave mixing in semiconductor photorefractive crystals may be utilized to suppress noise from scattering.³⁸ The orientation of the photorefractive crystal was chosen so that the diffracted signal of the counterpropagating reconstruction beam has its polarization rotated by 90° . The polarizing beamsplitter (PBS) increases the signal-to-noise ratio by selecting only the diffracted light and rejecting any s-polarized scattered light.

Degenerate four-wave mixing (DFWM) experiments were performed using the experimental setup shown in Fig. 7. This setup was used to measure diffraction efficiency, determine laser power requirements, and demonstrate image transfer. For diffraction efficiency measurements, the optical arrangement shown in the lower right circle of the figure and a single laser were used.

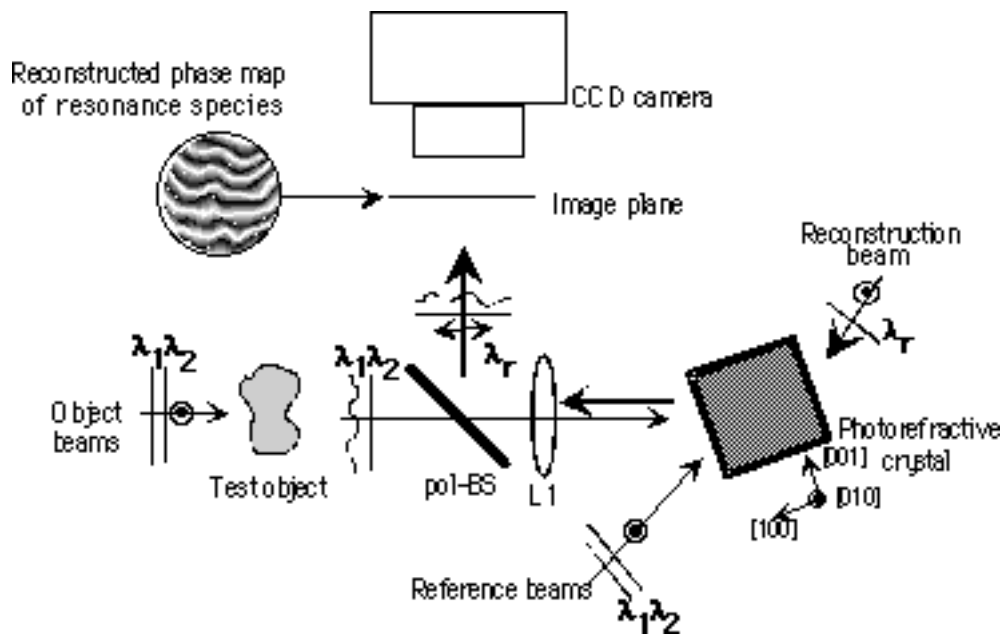


Figure 6. Phase conjugate configuration with polarization switching for real-time resonant holographic interferometry system.

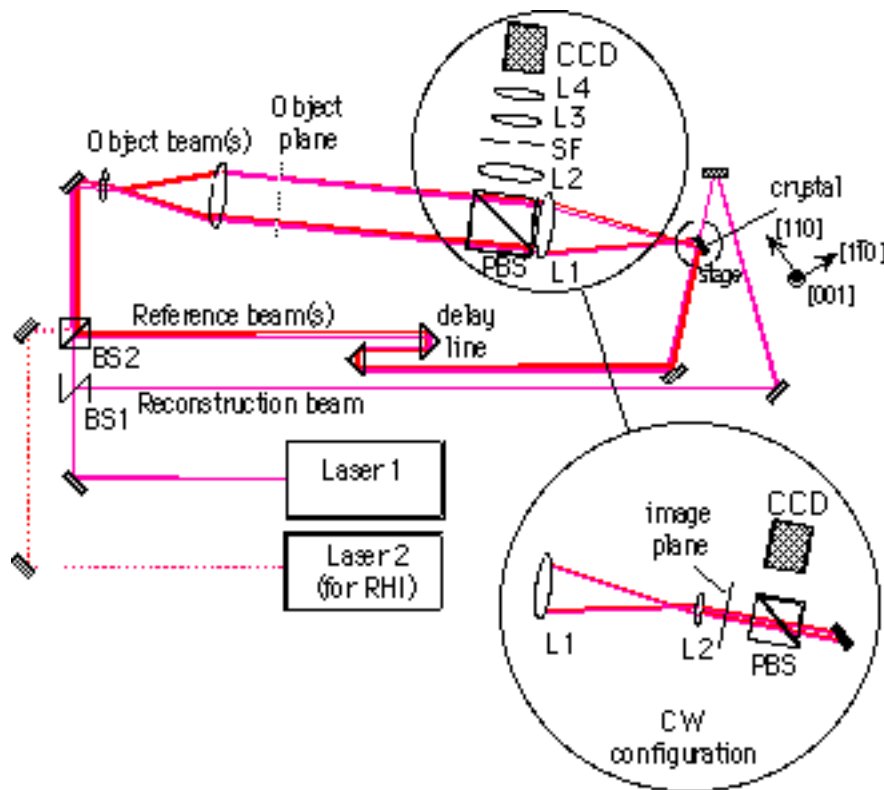


Figure 7. Optical arrangement for DFM and RHI experiments. Optics used for cw imaging experiments are shown as inset.

A separate reconstruction beam I_{rec} was used to mitigate aberrations from the crystal faces and to permit reconstruction at an angle slightly out of the plane of incidence. Reconstruction outside the plane of incidence facilitates spatial separation of the diffracted beam from reflections at the detector.

Demonstrations of real-time RHI measurements were performed using one of the strong potassium doublet absorption features (D_2) near 766 nm as our target. In addition to the simplified spectroscopy associated with probing alkali metal atoms, potassium seeding is useful for combustion studies because production of the neutral species

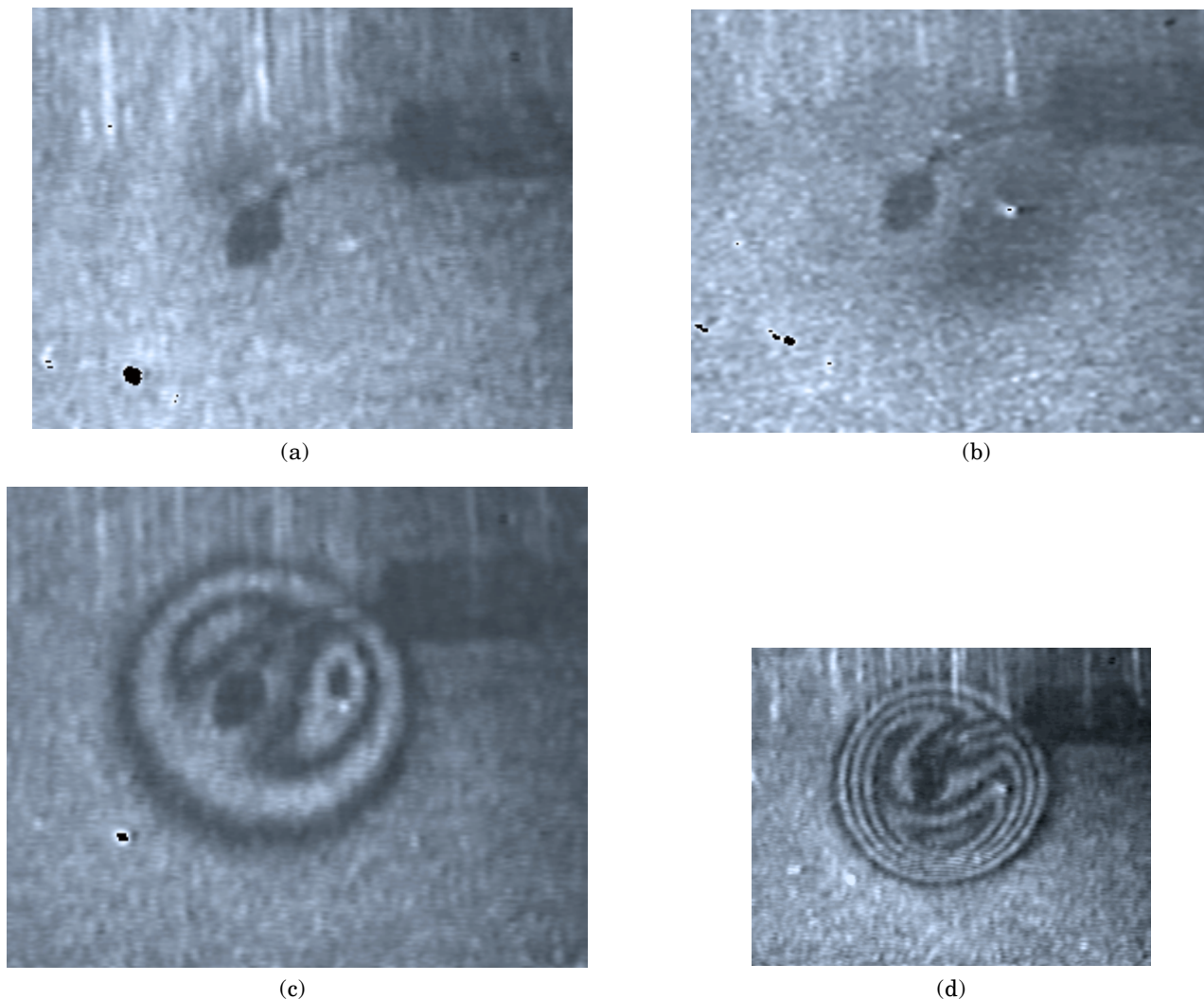


Figure 8. RHI interferograms of burning methanol droplets seeded with KCl. Each image is separated temporally by 100 ms.

(detected by RHI) occurs at the flame front. Thus, when used in conjunction with RHI, potassium seeding provides a method to track the time evolution of the flame front. Potassium may be conveniently seeded into combusting environments in such forms as potassium chloride (KCl).

Real-time RHI interferograms were recorded using the breadboard shown in Fig. 7. Dye lasers 1 and 2 were tuned 0.15 nm on either side of the D_2 absorption. Laser energies at the crystal were 1 mJ/pulse. Solutions of KCl in either water, methanol, or glycerol were introduced into various combusting environments including droplets suspended on fine wires, monodisperse droplet streams, and sprays.

Results are shown in Fig. 8 from experiments using single droplets on the order of 1 mm in diameter. The droplets were suspended from a fine wire and ignited with a butane lighter. After ignition, the butane lighter was removed and the droplet was allowed to burn on its own. The evolution of the combustion process was monitored at 10 Hz with the real-time RHI instrument. The figure shows a sequence of successive RHI interferograms of a KCl-seeded, burning methanol droplet. The images are separated by 100-ms intervals (10 Hz). Figure 8(a) shows the droplet just after ignition. The absence of fringes due to thermal gradients highlights the utility of holographic

optical background subtraction. In Fig. 8(b) a partial fringe is just visible in the lower right corner next to the droplet. In the subsequent frames, fringes are clearly visible. Such detail is not visible in images simultaneously recorded on conventional video because the flame luminosity totally obscures any detailed chemical and physical dynamics occurring at the thin flame front boundary. These images may reveal many of the finer details of the flame front development, and demonstrate that real-time RHI is a promising diagnostic tool for studying combusting droplets or other multiphase, highly luminous, highly scattering events.

For these demonstrations, the data framing rate was limited to 10 Hz by the laser system. The actual interferograms were recorded, reconstructed, and erased in a single 6-ns laser pulse. Therefore, the RHI instrument is ultimately capable of MHz data rates. To achieve higher data rates, laser pump sources with faster repetition rates and high-speed CCD cameras must be used. RHI interferograms of complex combusting sprays were also captured by injecting seeded water and methanol into an oxy/acetylene flame using an atomizer.

Under our test conditions, the interaction length was approximately 0.5 cm and the lasers were tuned ± 0.15 nm symmetrically about the absorption feature (absorption

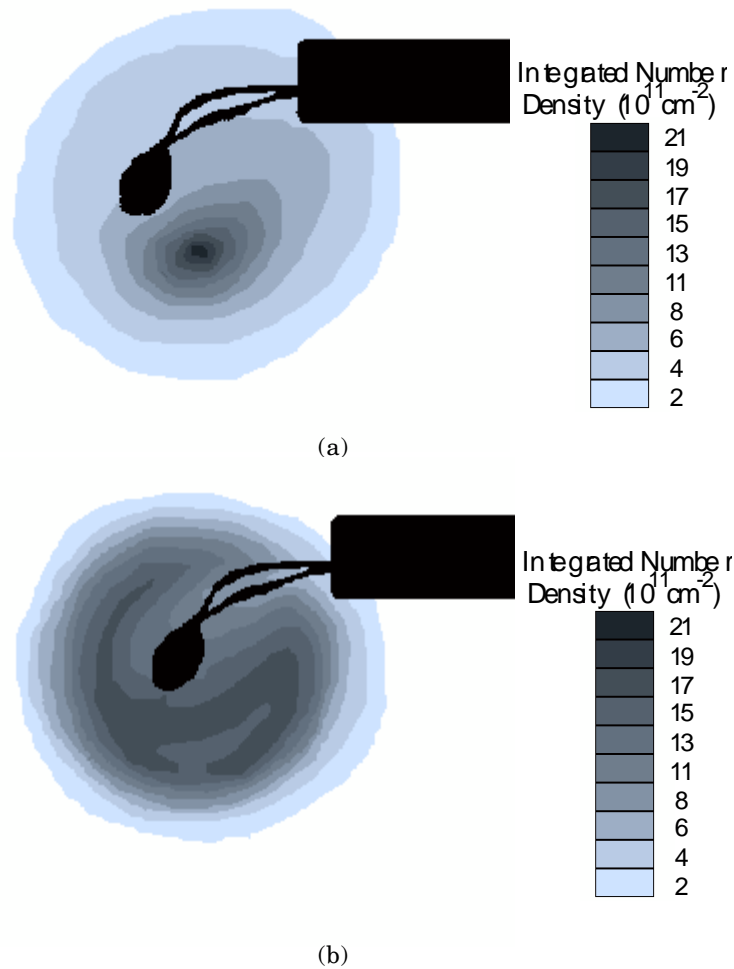


Figure 9. Potassium density maps produced from RHI interferograms: (a) shown in Fig. 8(c) and (b) shown in Fig. 8d. Values represent number density integrated along the line of sight ($L \approx 0.5 \text{ cm}$). Uncertainty in measurement is dominated by the fringe-tracking method $\sim 2 \times 10^{11} \text{ cm}^{-2}$.

line width = 0.024 nm). A minimum detectable concentration for our experiments was calculated to be $8.6 \times 10^{11} \text{ cm}^{-3}$, or 0.2 ppm. Analytical results predicted that the limit of fringe visibility was approximately 11 fringes, corresponding to a maximum measurable concentration of $N_{\text{max}} \leq 220 \text{ ppm}$. The observation of approximately five fringes in our experiments [see Figs. 8(c) and 8(d)] corresponds to a maximum concentration of 100 ppm. This sensitivity is comparable to that of FM diode laser spectroscopy, a single point, line-of-sight method.

To reduce the information contained in the RHI interferograms, we employed a manual fringe-tracking algorithm. This resulted in a resolution of approximately one-half of a fringe. Figure 9 shows gray-scale maps corresponding to path-length integrated number density for two RHI interferograms of potassium seeded into a methanol droplet. The density gradient spans an order of magnitude, which demonstrates excellent dynamic range. The uncertainty in the measurement is dominated by the fringe-tracking method that has on the order of one-half fringe resolution. Based on our estimates, the value of the maximum integrated number density, shown in the center of the interferogram, is $17 \pm 2 (10^{11} \text{ cm}^{-2})$.

Two-Color Contour Holography. The optical arrangement for the profilometer is shown in Fig. 10. A two-wave mixing geometry was used to record an initial

hologram at λ_1 . Because of the relatively slow response time of the crystal (tens of seconds for intensities used here), the laser could be rapidly tuned to a new wavelength λ_2 and used to reconstruct the stored holographic image before it was erased and rewritten. The reconstructed image interfered with the real-time image, produced by light reflected from the actual object, to generate contour interferograms. The contour interval could be tuned continuously and in real-time by changing the laser diode drive current. In addition, phase shifting for quantitative data reduction was accomplished by introducing a path length change in the reference beam.

The emission wavelength of diode lasers was tuned by controlling their temperature, drive current, or by using external feedback. In this manner, the wavelength can be controlled over a range of tens of nanometers. For our experiments, we used a diode laser with a maximum output of 30 mW and a nominal operating wavelength of 804 nm. The diode was thermally stabilized but had no external frequency stabilization. Wavelength tuning was accomplished by changing the laser drive current. The change in wavelength is given by

$$\Delta\lambda = \frac{\lambda^2}{c} \beta \Delta i, \quad (13)$$

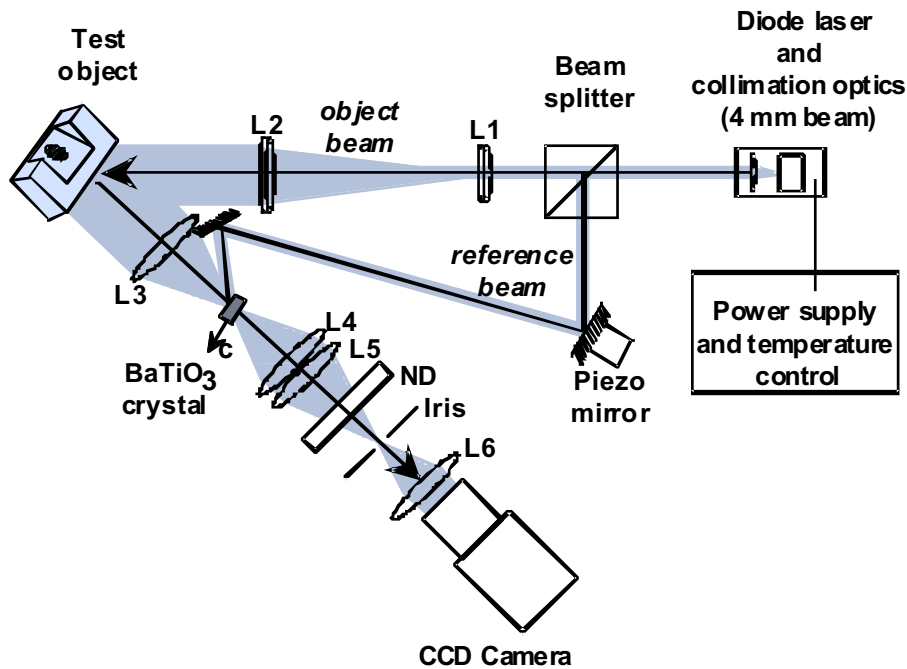


Figure 10. Two-color contour profilometer using BaTiO₃ and two-wave mixing geometry. L1: $f = 25.4$ mm, $d = 12$ mm; L2: $f = 160$ mm, $d = 40$ mm; L3: $f = 100$ mm, $d = 50$ mm; L4: $f = 100$ mm, $d = 50$ mm; L5: $f = 160$ mm, $d = 40$ mm; L6: $f = 31$ mm, $d = 16$ mm.

where λ is the nominal laser wavelength, c is the speed of light, Δi is the change in the drive current, and β is the so-called current-frequency modulation index. In a separate set of experiments, we measured $\beta = 3.0$ GHz/mA for our diode (Sharp OLT017). We also observed that the diode could be tuned over approximately 0.16 nm (25 mA) without a mode hop.

The BaTiO₃:Rh crystal (2400 ppm), which had dimensions of 3 (c axis) \times 3 \times 2 mm, was used for the experiment (Deltronic Crystals). The interaction length (2 mm) was intentionally kept short to permit Bragg matching over a wavelength shift of ~ 0.5 nm. The c axis of the crystal was parallel to the plane of incidence and the front and back faces were antireflection coated for 800-nm light. Both beams were p-polarized so that they coupled into the large r_{42} electro-optic coefficient of BaTiO₃. We measured a gain coefficient of 10 cm^{-1} at a wavelength of 804 nm with the object and reference beams incident at 20° and 45° with respect to the surface normal. The measured gain coefficient corresponds to a diffraction efficiency of approximately 28%. The two-wave mixing gain reached 90% of its steady-state value within 15 s at a combined beam intensity of 70 mW/cm^2 . By blocking the object beam and reducing the reference light, the grating could be readout for minutes.

Figure 11(a) shows a photograph of a wedge-shaped object used to test the profilometer system. The wedge was made of aluminum and was painted white for uniform reflectivity. Figure 11(b) shows a digitized interferogram where the contour interval was 2.1 mm ($\Delta i = 23.9$ mA). One fringe is visible across the top surface, indicating that the object was at a slight angle with respect to the contour reference plane. The contour interval could be continuously adjusted and viewed in real-time by changing the laser drive current. Fringe contrast could be adjusted by attenuating the object beam during playback; however, contrast was sufficient for data reduction without any changes in object intensity if the interferograms were recorded within several seconds.

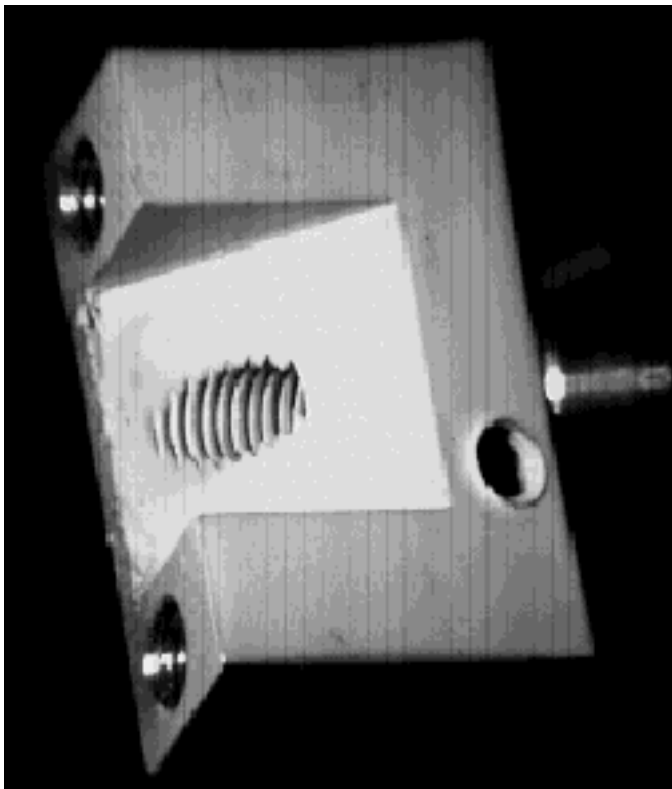
To produce quantitative data from the interferograms, we incorporated phase-shifting and phase-unwrap analysis software. Four interferograms with a phase shift of 90° between each were digitized and a wrapped phase map was generated using a standard algorithm.³⁹ Figure 11(c) shows a typical wrapped phase map.

A phase-unwrapping routine was used to produce a smooth image from the wrapped phase map. A ruler was imaged with the profilometer system and used to obtain scaling in the x-y dimension. The contour interval was calculated and used to convert gray scale to actual depth (z-dimension). The two-dimensional array of depth values were plotted as a 3-D wire frame in Fig. 11(d). The object height was within $\pm 100 \mu\text{m}$ of the dimensions measured using dial calipers.

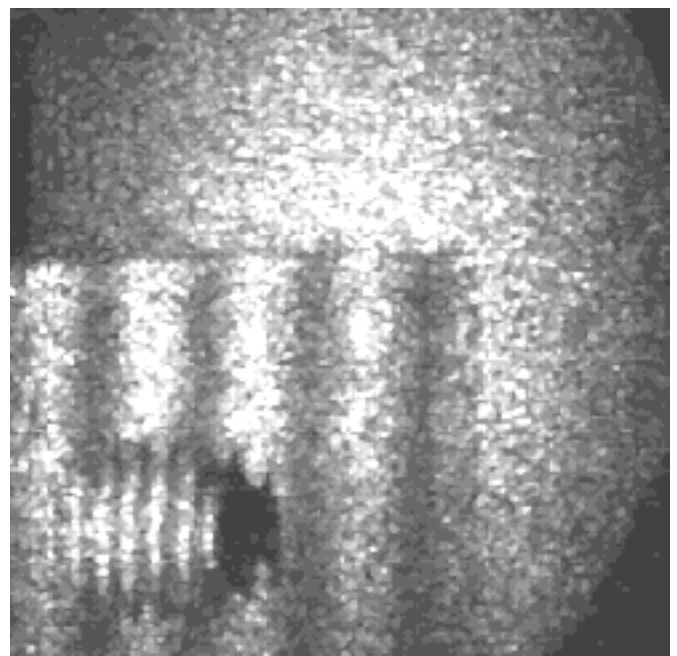
Conclusions

Holographic interferometry is a powerful method for obtaining quantitative information from holograms. The utilization of more than one wavelength of light during recording and/or the reconstruction process can produce a variety of diverse and powerful measurement techniques unique to the holographic approach. Three studies have been presented that demonstrate recent advancements in multicolor techniques. Each study demonstrated one of the three different methods outlined for utilizing multiple wavelengths (i.e., separately, creation of a synthetic wavelength, and direct interference). In each instance, the use of holography enhanced the use of interferometry, and in the case of RHI, holography produced a measurement that would have been impossible using traditional interferometry alone. \blacktriangle

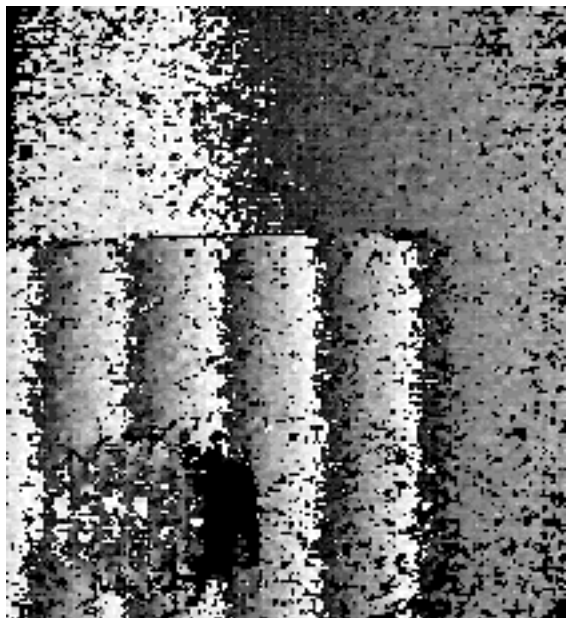
Acknowledgments. The authors wish to thank the many agencies and people who made the experimental programs discussed in this report possible. We wish to thank William Witherow at Marshall Space Flight Center for providing the laboratory facilities in which most of the TCHI experimentation was conducted and NASA for the



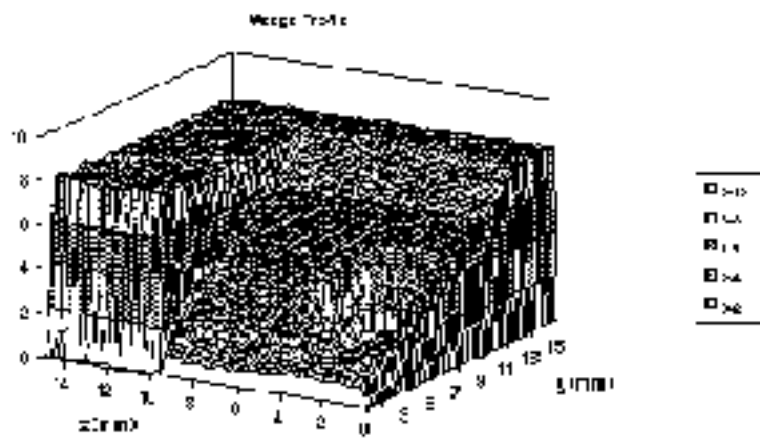
(a)



(b)



(c)



(d)

Figure 11. (a) Photograph of test object, (b) two-color holographic contour interferogram, (c) wrapped phase map, and (d) reconstructed 3-D model.

funding to do the work. We also appreciate the collaboration of Dr. Chandra Vikram throughout the program. With regard to the RHI material, the authors wish to thank Dr. Sudhir Trivedi of the Brimrose Corporation of America for providing the photorefractive crystal, Dr. D. Dunn-Rankin and Mr. R. Dimalanta for technical and laboratory assistance, and Drs. Peter DeBarber and Michael Brown from MetroLaser for their work and leadership. This work was partially supported by the National Science Foundation, the Air Force Geophysics Lab, the Army Research Office, and the Navy.

References

- M. H. Horman, An application of wavefront reconstruction to interferometry, *Appl. Opt.* **4**, 333–336 (1965).
- C. M. Vest, *Holographic Interferometry*, John Wiley & Sons, New York, 1979.
- J. D. Trolinger, Fundamentals of Interferometry and Holography for Civil and Structural Engineering Measurements, *Opt. Las. Eng.* **24**, 89–109 (1996).
- P. Gill, Laser interferometry for precision engineering metrology, in *Optical Methods in Engineering Metrology*, D.C. Williams, Ed., Chapman and Hall, London (1993) p. 153
- J. E. Grievenkamp and J. H. Bruning, in *Phase Shifting Interferometry*, Daniel Malacara, Ed., Wiley Interscience Optical Shop Testing, 1992, p. 501.
- G. E. Sommergren, Optical Heterodyne Profilometry, *Appl. Opt.* **20**, 610 (1981).
- R. Johnston and K. Grace, Refractive index detector using zeeman interferometry, *Appl. Opt.* **29**, 4720 (1990).
- G. V. Dreiden, et al, Plasma diagnostics by resonant interferometry and holography, *Sov. J. Plasma Phys.* **1**, 256 (1975).
- J. E. Millerd and N. J. Brock, Holographic profilometry with a rhodium-doped barium titanate crystal and a diode laser, *Appl. Opt.* (in press).
- Y.-S. Kuo, K. Choi, J. K. McIver The effect of pump bandwidth, lens focal length, and lens focal point location on stimulated Brillouin scattering threshold and reflectivity, *Opt. Commun.* **80**, (3/4) 233–238 (1991).
- N. A. Riza Scanning heterodyne optical interferometry, *Rev. Sci. Instrum.* **67**(7) (1996).
- J. T. Evans, Real time metrology using heterodyne interferometry, *Proc. SPIE* **429**, 199 (1983).
- G. E. Sommergren, Optical heterodyne profilometry, *Appl. Opt.* **20**, 610 (1981).
- J. D. Trolinger, Ultra high resolution interferometry, *Proc. SPIE* **2861**, 114–123 (1996) *Laser Interferometry VIII: Techniques and Analysis*.
- J. D. Trolinger and Neal Brock Sandwich, double reference wave, holographic, phase-shift interferometry, *Appl. Opt.* **34**, 6354 (1996).
- D. C. Weber, J. D. Trolinger, C. S. Vikram, W. K. Witherow, *Appl. Opt.* (in press).
- F. Mayinger and W. Panknin, "Holographic two-wavelengths interferometry for measurement of combined heat and mass transfer," in *Combustion Measurements: Modern Techniques Instrumentation*; Proc. SQUID Workshop, (A77-33701 15-35) Academic Press, Inc., New York, Hemisphere Publishing Corp., Washington, D.C., p. 270, 1976.
- A. Ecker, Two-wavelength holographic measurement of temperature and concentration during alloy solidification, *J. Thermophys. Heat Transfer* **2**, 193 (1988).
- A. Ecker, A two wavelength holographic technique simultaneous measurement of temperature concentration during the solidification of two component systems, *AIAA* **6**, ESA-supported research, 1987.
- G. V. Dreiden, A. N. Zaidel, G. V. Ostrovskaya, Y. I. Ostrivskii, N. A. Pobedonostseva, L. V. Tanin, V. N. Filippov and E. N. Shedova, Plasma diagnostics by resonant interferometry and holography, *Sov. J. Plasma Phys.* **1**, 256 (1975).
- L. F. Rubin and D. M. Swain, Near-resonant holography, *Opt. Lett.* **16**, 526 (1991).
- J. Millerd, N. Brock, M. Brown, and P. DeBarber Real-time resonant holography using bacteriorhodopsin thin films, *Opt. Lett.* **20**, 626 (1995).
- G. Valley, J. Dubard, A. Smirl, and A. M. Glass, Picosecond photorefractive response of GaAs:EL2, InP:Fe, and CdTe:V, *Opt. Lett.* **14**, 961 (1989).
- J. P. Huignard and J. P. Herriau, Real-time double exposure interferometry with Bi₁₂SiO₂₀ crystals in transverse electro-optic configuration, *Appl. Opt.* **16**, 1807 (1977).
- F. M. Kuchel and H. J. Tiziani, Real-time contour holography using BSO crystals, *Opt. Commun.* **38**, 17 (1981).
- M. P. Petrov, S. I. Stepanov, and A. V. Khomenko, *Photorefractive Crystals in Coherent Optical Systems*, Springer-Verlag, New York, Chap. 9 pp. 173–181, Chap. 5, p. 85–87 and Chap. 2, pp. 20–23 (1991).
- J. Frejlich, A. A. Kamshilin, V. V. Kulikov, E. V. Mokrushina, Adaptive holographic interferometry using photorefractive crystals, *Opt. Commun.* **70**, 82–86 (1989).
- R. Magnusson, X. Wang, A. Hafiz, T. Black, L. Tello, A. Haji-shelkh, S. Konecni, and D. Wilson, Experiments with photorefractive crystals for holographic interferometry, *Opt. Eng.* **33**, 596 (1994).
- M. Ziari, W. Steier, P. Ranon, S. Trivedi, and M. B. Klein, Photorefractivity in vanadium-doped ZnTe, *Appl. Phys. Lett.* **60**, 1052 (1992).
- J. Millerd, A. Partovi, and E. Garmire, Near resonant photorefractive effects in bulk semiconductors, Chapter 6, *Photorefractive Effects and Materials*, D. Nolte, Ed., Kluwer Academic Publishing, London, 1995.
- K. Haines and B. P. Hildebrand, Contour generation by wavefront reconstruction, *Phys. Lett.* **19**, 10 (1965).
- A. A. Friesem, U. Levy, and Y. Silberberg, Real-time holographic contour mapping with dye lasers, in *The Engineering Uses of Coherent Optics*, E. R. Robertson, Ed., Cambridge University Press, Cambridge, 353–373, 1976.
- F. M. Kuchel and H.J. Tiziani, Real-time contour holography using BSO crystals, *Opt. Commun.* **38**, 17–21 (1981).
- P. Tatam, J. Davies, C. Buckberry, and J. Jones, Holographic surface contouring using wavelength modulation of laser diodes, *Opt. Laser Technol.* **22**, 317 (1990).
- Y. Zou, G. Pedrini, and H. Tiziani, Surface contouring in a video frame by changing the wavelength of a diode laser, *Opti. Eng.* **35**, 1074 (1996).
- B. A. Wechsler, M. B. Klein, C. C. Nelson and R. N. Schwartz, Spectroscopic and photorefractive properties of infrared-sensitive rhodium-doped barium titanate, *Opt. Lett.* **19**, 536 (1994).
- W. Osten, W. Nadeborn, and P. Andra, "General hierarchical approach in absolute phase measurement," *Laser Interferometry VIII: Techniques and Analysis*, *Proc. SPIE* **2860**, 2 (1996).
- G. Gheen and L. Cheng, Image processing by four wave mixing in photorefractive GaAs, *Appl. Phys. Lett.* **51**, 1481 (1987).
- D. W. Robinson and G. T. Reid, Eds., *Interferogram Analysis*, IOP Publishing Ltd., Bristol (1993).